Biointerface Research in Applied Chemistry
Open-Access Journal (ISSN: 2069-5837)

Article
Volume 14, Issue 3, 2024, 68
https://doi.org/10.33263/BRIAC143.068

Polymeric Silver Nanoparticles for ACE2-Receptor Targeting to Lung Cancer Cells *in Vitro*

Dillon Sivalingam [1], Moganavelli Singh [1,*]

1. Nano-Gene and Drug Delivery Group, Discipline of Biochemistry, University of KwaZulu-Natal, Private Bag X54001, Durban, South Africa
* Correspondence: singhm1@ukzn.ac.za;

Scopus Author ID 3709591900
Received: 13.08.2023; Accepted: 16.11.2023; Published: 17.02.2024

Abstract: Lung cancer is a major cause of cancer-related deaths globally. This study aims to target the overexpressed angiotensin-converting enzyme 2 (ACE2) receptor in lung cancer using cisplatin (CIS)-conjugated silver nanoparticle (AgNP)-based drug delivery system. AgNPs were synthesized and coated with a chitosan (CS) polymer and the SARS-CoV-2 receptor binding domain (SCRBD) targeting ligand and were assessed in vitro for ACE2 receptor targeting in a lung cancer cell model. The AgCS-CIS-SCRBD nanocomplex exhibited 61% CIS encapsulation with a pH-dependent drug release over 72 hours. Characterization using Fourier transform infrared (FTIR), UV-visible spectroscopy, dynamic light scattering (DLS), and transmission electron microscopy (TEM) confirmed the synthesis, functionalization, morphology (spherical), size (<150nm), and stability (>15mV) of the NPs and nanocomplexes. Cytotoxicity studies revealed significant levels of cell death in the lung cancer (A549) cells, with the non-cancer human embryonic kidney (HEK293) cells displaying lower cytotoxicity. The receptor competition binding assay confirmed the specificity of the bound SCRBD ligand (AgCS-CIS-SCRBD nanocomplex) for the ACE2 receptor. The AgCS-CIS-SCRBD nanocomplex exhibited apoptotic effects on the A549 cells with acceptable apoptotic indicesThese results highlight the potential of this novel AgCS-CIS-SCRBD nanocomplex in the targeted delivery of CIS for lung cancer therapy.

Keywords: ACE2; cisplatin; drug delivery; lung cancer; silver nanoparticles; receptor targeting.

1. Introduction

Lung cancer is a heterogeneous disease and is causing most of the cancer-related deaths across the continent [1]. It is a commonly diagnosed cancer in both males and females, with recent trends showing an increase among females [2,3]. Many studies have reported the expression of the angiotensin-converting enzyme 2 (ACE2) in lung cancer. The ACE2 receptor has gained much popularity since it has been identified as the primary receptor for entry of the 2020 novel coronavirus [4,5], also known as COVID-19, with a myriad of studies reporting that lung cancer patients have a greater risk of contracting COVID-19 due to the upregulated expression of ACE2 in lung cancer cells [6-8]. In healthy lung tissue, ACE2 is reported to be moderately expressed [9].

ACE2 is a zinc-type I carboxypeptidase commonly known for regulating the renin-angiotensin system (RAS) [5]. Studies have reported that the variation in the expression level of ACE2 can either reduce or inhibit the endothelial growth factor, metastasis, tumor development, and cancer angiogenesis or induce metastasis and cancer cell proliferation [7,10-

12]. The overexpression of ACE2 creates an exciting avenue in nanomedicine for developing novel targeted nano-drug delivery systems that can utilize ACE2 as a target. Such delivery systems could potentially provide a new approach to cancer therapies in the battle against lung cancer. Innovative approaches using target-specific delivery systems have shown much promise in increasing a drug's therapeutic efficacy while improving patient compliance [13,14]. When drugs are administered in their free form, they are often inactivated, metabolized, or degraded in the system., while also eliciting unpleasant side effects in patients [15]. Nanoparticle (NP)--based drug carriers have the potential to overcome physiological barriers, protect the drug, and target it to the desired diseased site, thereby reducing much of the challenges faced by traditional drug delivery.

Silver NPs (AgNPs) have been utilized in biomedicine, pharmaceuticals, waste disinfection, and drug delivery and have shown to have better physical, chemical, and biological properties than their bulk form. Silver is a lustrous, ductile, and malleable metal that is chemically inactive and stable in water. It is an abundant natural resource that does not oxidize in the presence of air [16,17]. Its properties range from ease of synthesis, chemical stability, biocompatibility, optical, thermal, and electrical conductivity to anti-viral, anti-inflammatory, antifungal, antibacterial, anticancer, anti-angiogenic, and catalytic properties [18-22]. These properties make AgNPs interesting therapeutic nanocarriers. However, AgNPs have been prone to toxicity, which limits their use in nanomedicine. Xu et al. (2020) summarized the potential toxicities of AgNPs *in vitro* and *in vivo*, showing that most of these are concentration- or dose-dependent. Factors such as size, shape, exposure time, functionalization, and surface charge were crucial in modulating toxicity [23].

Positively charged NPs are considered suitable for medical applications due to their good cellular uptake [24]. AgNPs are usually negatively charged and require functionalization with suitable bio-molecules, such as cationic polymers, that will imbue the NPs with a positive charge [25]. Polymers offer biocompatibility, reduced toxicity, controlled drug release, enhanced therapeutic binding, and improved cell membrane interactions. Chitosan is a cationic polymer produced from the deacetylation of the polysaccharide chitin [26,27]. Chitosan is a non-toxic, biodegradable, and biocompatible polymer that exhibits no side effects, aids in controlled drug release, conveys stability to NPs, and allows for the conjugation of hydrophobic and hydrophilic drugs [27-29]. AgNP functionalization with chitosan can have a dual function by reducing the cytotoxicity of the AgNPs and improving their drug delivery, making chitosan a polymer of choice in many delivery systems.

The ACE2 receptor makes an exciting target for cancer research, and to the best of our knowledge, targeting ACE2 specifically for lung cancer therapy has not yet been reported. The moderate expression of ACE2 in healthy lung cells and overexpression in cancer cells justifies the strategy for therapeutic targeting of lung cancer cells via the ACE2 receptor. This study aims to synthesize, characterize, and evaluate the anticancer activity of an ACE2 receptor-targeted–AgNP-based drug delivery system in the A549 lung cancer cell model.

2. Materials and Methods

2.1. Materials.

Silver nitrate (AgNO3, Mw:169,87 g/mol), chitosan ≥ 75% deacetylated (Mw: 150000-200000Da), sodium tripolyphosphate (TPP, Mw: 326.86g/mol), (acridine orange (Mw:

265.36g/mol), dialysis tubing (12000Da MWCO), 1-ethyl-3-(3-dimethyl aminopropyl) carbodiimide (EDC), N-hydroxysuccinimide (NHS), and Recombinant 2019-NCOV Spike S1 protein or SARS-CoV-2 Receptor Binding Domain) were supplied by Sigma Aldrich Chemical Co., (St. Louis, MO, USA). Phosphate-buffered saline (PBS, 140mM NaCl, 10mM phosphate buffer, 3mM KCl), tri-sodium citrate (Mw: 294.10 g/mol), ethidium bromide, 3-(4,5-dimethylthiazol-2-yl)-2,5-diphenyl tetrazolium bromide (MTT), and cisplatin (Mw: 300g/mol) were provided by Merck (Darmstadt, Germany). The human embryonic kidney (HEK293) and lung adenocarcinoma (A549) cells were originally sourced from the American-type culture collection in Manassas, VA, USA, and used in passage 2. Hyclone GE Healthcare (Utah, USA) supplied the sterile fetal bovine serum (FBS). Eagle's Minimum Essential Medium (EMEM) with L-glutamine (4.5g/mL), penicillin/ streptomycin/ amphotericin B (100 x) antibiotic mixture [Amphotericin B (25µg/mL), penicillin (10 000 Units/mL), streptomycin sulfate (10 000µg/mL)] and trypsin-versene mixture, were supplied by Lonza BioWhittaker (Verviers, Belgium). All sterile tissue culture plasticware was purchased from Corning Inc. (New York, USA). Analytical grade reagents and ultrapure (18MOhm) water (Milli-Q Academic, Millipore, France) were used in all experiments.

2.2. Synthesis of silver nanoparticles (AgNPs).

The Turkevich method was adapted to synthesize the AgNPs [30]. To 50mL of distilled water was added 8.5mg of $AgNO_3$, under constant stirring and heating to 95°C. After that, 5mL of trisodium citrate (1%) was added dropwise with stirring, and the solution was heated for 10min. A color change from clear to dark yellow was observed as the AgNPs were formed. The mixture was then removed from heating and allowed to cool in the dark at room temperature.

2.3. Functionalization of AgNPs with chitosan.

Approximately 1.25mL of trisodium polyphosphate (TPP) (0.74mg/mL) was added to 2.5mL of chitosan (1 mg/mL in 2% acetic acid, pH 4.5) with stirring. After 3h, 2.5mL of the AgNPs was added dropwise at 15-second intervals. This was stirred overnight, followed by centrifugation of the chitosan-AgNPs (AgCS) mixture at 3200rpm for 15min. The pellet was resuspended in 5mL distilled water, sonicated for 20min, and stored in the dark at 4°C.

2.4. Formulation of cisplatin-loaded chitosan-AgNPs (AgCS-CIS).

With stirring, approximately 2.5mL of the chitosan stock was added dropwise to 1.25mL TPP. After that, 57.5µL of cisplatin (2.5mg/mL in DMF) was added, and the mixture was stirred over 24h. Approximately 2.5mL of AgNPs was added dropwise at 15-second intervals, and the mixture was stirred overnight and centrifuged as previously.

2.5. SARS-CoV-2 receptor binding domain conjugation to AgCS-CIS (AgCS-CIS-SCRBD).

To 1mL of the SARS-CoV-2 receptor binding domain (SCRBD), ligand stock solution (0.01µg/mL) was added 0.4mL of EDC (0.375mg/mL) and NHS (0.3mg/mL) with stirring for 24h. After that, 1.25mL TPP, 2.5mL chitosan, and 57.5µL of cisplatin were added, and the mixture was stirred overnight. Approximately 2.5mL of the AgNPs was added dropwise, and the mixture was stirred for 24h, followed by centrifugation as previously.

2.6. Ultraviolet-visible (UV-vis) and Fourier transform infrared (FTIR) spectroscopy.

The maximum wavelength for the absorption of the AgNPs and nanocomplexes was assessed using a UV-vis spectrophotometer (Jasco V-730, Hachioji, Japan) over a wavelength range of 300- 600nm. AgNPs have an extraordinary plasmon resonance, and the UV peak observed correlates to the NP's size and shape. This method was further used to determine the successful synthesis and modification of the AgNPs, as indicated by shifts in the maximum absorption spectral peaks of the different AgNPs.

FTIR aids in establishing the existence of essential groups and bonds in a sample by visualizing specific peaks. The liquid samples were freeze-dried overnight, and attenuated total reflection-FTIR spectroscopy was conducted using samples in a powder form. The spectrum was run at 25°C in a 4000–400cm^{-1} wavelength range using 1mg of sample in a Spectrum 100 Perkin Elmer FTIR spectrophotometer equipped with Spectrum Analysis Software.

2.7. Transmission Electron Microscopy (TEM).

The respective AgNPs and nanocomplexes (50µL) were placed on 400-mesh carbon-coated copper grids (Ted Pella Inc. Redding, USA) and dried for 1 h at room temperature. The samples were visualized utilizing a JEOL-JEM T1010 (Jeol, Tokyo, Japan) electron microscope without warming at -150°C, an acceleration voltage of 100kV, and a magnification of 60 000x. Images were obtained using iTEM Soft Imaging Systems (SIS) Megaview III fitted with a side-mounted 3-megapixel digital camera.

2.8. Particle size and zeta potential analysis.

The sizes, polydispersity index, and zeta potentials for all AgNPs and nanocomplexes were measured using dynamic light scattering (DLS) in a Malvern Zetasizer Nano-ZS (Malvern Instruments Ltd., Worcestershire, UK). All measurements were conducted at room temperature utilizing DTS0012 disposable polystyrene cuvettes. Measurements were performed in triplicates, and approximately 1mL of a 1:500 dilution (in water) of each sample was assessed.

2.9. Cisplatin encapsulation efficiency (EE).

An indirect analysis method was employed to calculate the amount of bound drug in the nanocomplex based on the principle that higher molecular weight NPs will sediment under centrifugal forces compared to the free drug, which will remain in the supernatant. The amount of unbound drug was measured by centrifugation of the sample at 3200rpm for 15min, collecting the supernatant, and measuring the UV absorbance at 298nm to determine the amount of unbound cisplatin. The EE was estimated using equation 1 below:

$$EE\ (\%) = cisplatin\ total - cisplatin\ supernatant/cisplatin\ total \times 100 \quad (1)$$

2.10. Drug release studies.

The drug release profiles of the nanocomplexes were determined for 72h under varying pH conditions (pH 4.5, 6.0, and 7.4). Approximately 1mL of each nanocomplex (AgCS-CIS and AgCS-CIS-SCRBD) were dialyzed (MWCO 12000Da) against PBS (5mL) for 72h at 37°C. A 10µL sample was removed at regular intervals, and the amount of cisplatin released was determined by UV-vis spectroscopy at 298nm. Measurements were done in triplicate to

generate a drug release profile for the respective nanocomplexes under the different pH conditions against time.

2.11. MTT cytotoxicity assay.

The cytotoxicity of the free drug cisplatin, AgNPs, and drug nanocomplexes was evaluated utilizing the MTT cytotoxicity assay. The HEK293 and A549 cells were seeded into 96-well plates at a density of 2.4 x 10^4 cells/well. Cells were incubated at 37°C overnight to allow for attachment. After that, the media was replaced with 100µL of fresh media, followed by the addition of 5µg, 10µg, 15µg, 25µg, and 50µg of the nanocomplexes (AgNP, AgCS, AgCS-CIS, and AgCS-CIS-SCRBD) and the free drug (cisplatin) in triplicate, into separate wells. A positive control containing untreated cells was set as 100% cell survival. After incubation of the cells at 37°C for 48h, the medium was replaced with a fresh medium (100µL) containing 10% MTT solution (5mg/mL in PBS). This was incubated for 4h, followed by the aspiration of the MTT-medium from wells and the addition of 100µL of DMSO to solubilize the formazan crystals produced. Absorption was read at 570nm (Mindray MR-96A microplate reader, Vacutec, Hamburg, Germany) using DMSO as a blank. The cell viability was determined using equation 2.

$$\%\ Cell\ viability\ =\ Abs\ of\ treated\ -\ Abs\ of\ control\ /Abs\ of\ control\ x\ 100 \quad (2)$$

2.12. Receptor binding assay.

This assay confirmed the mechanism of the uptake of the AgCS-CIS-SCRBD nano-complex by the 549 cells. Confluent A549 cells were seeded and incubated as previously. The medium was then replenished, and excess SCRBD (80µg) was added to the cells. The cells were then incubated for 1 h at 37°C to allow the free SCRBD to bind to their cognate receptors on the A549 cells. After that, AgCS-CIS-SCRBD, at concentrations of 25µg/100µL and 50µg/100µL, were added to the cells and incubated at 37°C for 48 hours. After the aspiration of the medium, the cells were treated as done for the MTT assay (section 2.11).

2.13. Apoptosis assay.

Cells were seeded and incubated as previously. Following incubation, the media was replaced with 100µL of fresh media. The nanocomplexes (AgCS-CIS and AgCS-CIS-SCRBD) at their IC50 concentrations and the free drug, cisplatin, were added into their respective wells. The assay was done in triplicate. A positive control of untreated cells was included. The cells were incubated for 48h at 37°C. After that, the medium was removed from the wells. The cells were washed with 100 µL of PBS and added 15µL of the dual acridine orange and ethidium bromide dye solution (1:1 w/w, 100mg/mL in PBS). The plate was then gently shaken for 5 min, and the excess dye was removed by washing twice with PBS. The cells were viewed under an Olympus CKX41 fluorescence microscope (Olympus Co., Tokyo, Japan) at 200x magnification. The apoptotic index (AI) was calculated by dividing the number of apoptotic cells observed by the total number of cells.

2.14. Statistical analysis.

All the data in the study are presented as means ± standard deviation (±SD n=3). A two-way ANOVA was used for the MTT and receptor binding assays. The statistical significance of all tests was set at ****p<0.00001. Each experimental value was compared to its corresponding control. GraphPad Prism 2022 was used.

3. Results and Discussion

3.1. UV-visible and FTIR spectroscopy.

The synthesis and modification of the AgNPs were initially confirmed using UV-vis spectroscopy (Figure 1) within a 300–600nm range.

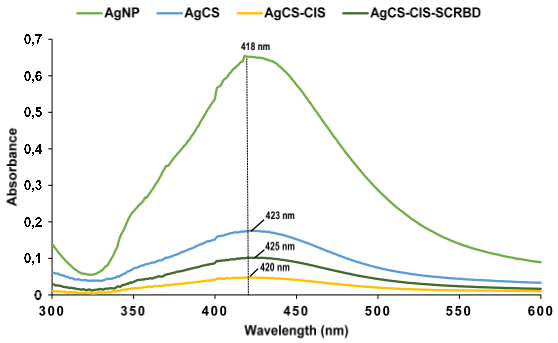

Figure 1. The UV-vis spectra of AgNP, AgCS, AgCS-CIS, and AgCS-CIS-SCRBD.

The successful synthesis of the AgNPs was noted as a single peak at 418nm. This peak wavelength correlates to previous studies of small-sized NPs [31-33], and being a single peak also confirmed that there were no by-products [34]. The successful functionalization of the AgNPs with the chitosan polymer was confirmed by a redshift, with a λmax at 423nm. A blueshift from 423nm to 420nm indicated the binding of the anticancer drug cisplatin to the NPs, successfully forming the AgCS-CIS nanocomplex.

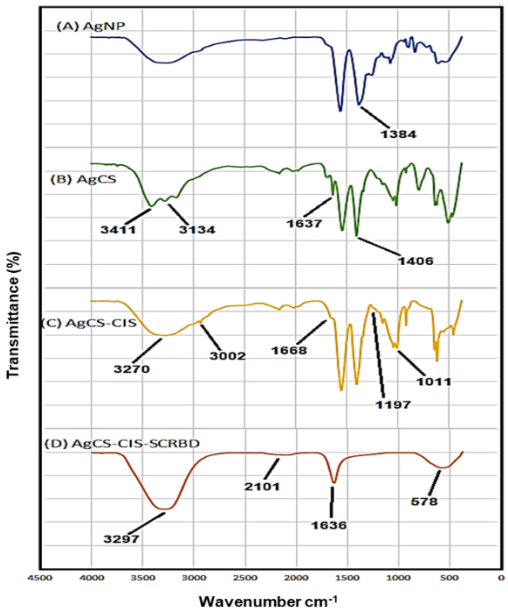

Figure 2. FTIR Spectra of **(A)** AgNP; **(B)** AgCS; **(C)** AgCS-CIS; **(D)** AgCS-CIS-SCRBD.

The conjugation of the targeting ligand to the nanocomplex was suggested by a redshift from 423nm to 425nm. The peak shifts also suggested an increased particle size, which can be expected due to functionalization.

FTIR further confirmed the synthesis and functionalization of the AgNPs by the presence of the essential functional group/s characteristic of each NP (Figure 2).

The FTIR spectra (Figure 2 A) showed a vibrational stretch of 1384cm^{-1} falling within 1400–1200cm^{-1}, characteristic of a nitro compound (NO_2) attributed to the $AgNO_3$ starting material for the AgNP synthesis. Figure 2B shows a shift in this peak to 1406cm^{-1}, suggesting the encapsulation of the AgNPs by chitosan [25]. Peaks between 1151cm^{-1} to 922cm^{-1} are the skeletal vibrations involving the C-O stretching [35]. The amide from chitosan is apparent at an absorption peak of 1637 cm^{-1}. The peaks at 3411cm^{-1} (N-H vibrational stretch) and 3134cm^{-1} (O-H vibrational stretch) correspond to chitosan [25]. Figure 2 C displays a peak at 3270cm^{-1} within the 3200cm^{-1} to 3280cm^{-1} regions, revealing an amide stretch for cisplatin [36,37]. Peaks within the 1200cm^{-1} and 1000cm^{-1} regions suggest the NH^{3+} and C-O stretching from chitosan. The peak at 1197cm^{-1} illustrates the symmetrical amide binding of cisplatin, while the peak shift from 1637cm^{-1} to 1668cm^{-1} signifies the conjugation of cisplatin to the chitosan polymer. The absorption bands at 1011cm^{-1} and 3002cm^{-1} further reveal the presence of the N-H and C-O stretching for the chitosan conjugated to cisplatin. Figure 2D represents the targeting nanocomplex that contains the SCRBD ligand. A peak at 1636 cm^{-1} suggests the presence of chitosan. The peak at 2101cm^{-1} suggests a terminal alkyne [38]. The peak (2101cm^{-1}) within the 2140–1990cm^{-1} region indicates the N=C=S stretching [39] of the amino acids in the SCRBD ligand. The peak at 3297cm^{-1} falls within the 3550–3200cm^{-1}, 3333-3267cm^{-1}, and 3280-3200cm^{-1} regions, suggesting an O-H, C-H, and amide stretching [36,37,39]. There were no distinctive peaks for the AgNPs. Studies have reported that proteins bind to NPs via amide groups [40], as with the SCRBD ligand. The peak at 578 cm^{-1} falls within the 690–515 cm^{-1} and 600–500cm^{-1} regions, suggesting C-Br and C-I stretching [39], which could also be associated with the amino acid groups in the SCRBD ligand

3.2. Transmission electron microscopy (TEM).

TEM images revealed NPs that were spherical with uniform particle size distributions.

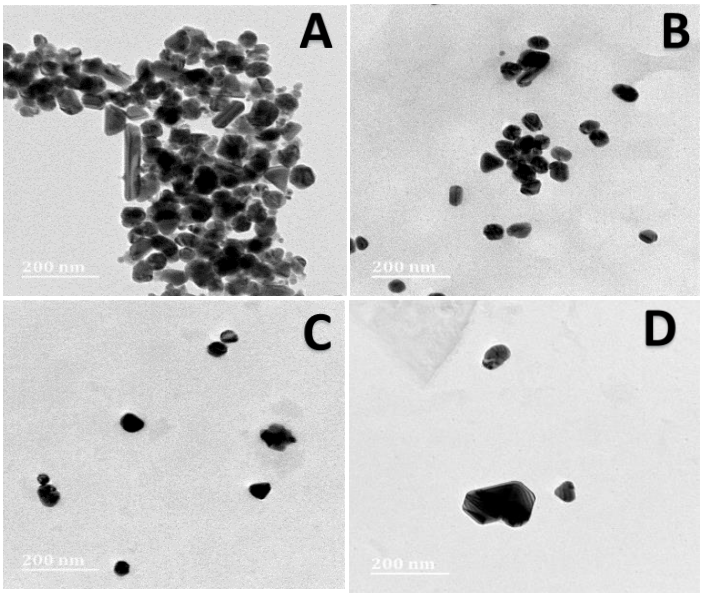

Figure 3. TEM micrographs of **(A)** AgNP; **(B)** AgCS; **(C)** AgCS-CIS; **(D)** AgCS-CIS-SCRBD.

The unmodified AgNPs (Figure 3 A) showed evidence of some aggregation compared to the AgCS (Figure 3B), AgCS-CIS (Figure 3C), and AgCS-CIS-SCRBD (Figure 3D) that displayed a more monodisperse population compared. The NP particle sizes from TEM ranged from 40-110nm.

Based on the method adapted to synthesize the AgNPs, it is common to observe aggregation of the unmodified AgNPs under TEM. The improved particle distribution of the modified AgNPs can be attributed to the presence of the chitosan polymer, which acted both as a stabilizing and a capping agent. Similar results have been reported previously for Ag and AgCS NPs, but with a smaller particle size range [34].

3.3. Particle size and zeta potential analysis.

Dynamic light scattering (DLS) was employed to estimate the hydrodynamic sizes to provide a more accurate determination of size, which is in keeping with what would be observed in vivo. DLS provided details on the stability and size distribution of the NPs and nanocomplexes and confirmed the successful binding of the polymer, drug, and ligand to the AgNPs. Table 1 summarizes the size distributions, zeta potentials, and polydispersity indices (PDI) of the NPs and nanocomplexes.

Table 1. Size distributions and zeta potentials of AgNPs and nanocomplexes obtained from dynamic light scattering (DLS).

Nanocomplex	Size (nm)	PDI	Zeta (mV)
AgNPs	31.6± 3.327	0.292± 0.096	-30.8± 0.866
AgCS	148.87± 6.834	0.183± 0.069	20.3± 0.551
AgCS-CIS	108.66± 19.33	0.140± 0.119	22.8± 1.61
AgCS-CIS-SCRBD	133± 10.09	0.193± 0.076	21.1± 0.954

NP sizes increased from 31.6nm for the AgNPs to 148.87nm upon chitosan functionalization (AgCS) but decreased to 108.66 nm upon cisplatin encapsulation. With the addition of the ligand, the nanocomplex size increased to 133nm. In theory, the chitosan matrix will entrap the ligand and cisplatin molecules and cause an increase in NP size upon functionalization. However, a decrease in nanocomplex size upon cisplatin conjugation was noted and is in keeping with that previously reported [25]. It should be noted that sizes obtained from TEM and NTA usually differ. This is attributed to the methods used for the preparation of the samples. For TEM the samples are in a dehydrated state, while for NTA the samples are measured in aqueous media (in this study, ultrapure water was used). The latter provides a hydrodynamic size that includes the core of the NP and the swollen corona, which swells under aqueous conditions [28,41]. Importantly, all the NPs and their drug nanocomplexes were below 150nm. Although 50 or 100nm may be regarded as an upper limit for cellular uptake, larger NPs can efficiently enter cells via caveolin or clathrin-mediated endocytosis or phagocytosis, which enables the uptake of particles of up to 250nm [42,43]. Importantly, it was suggested that smaller AgNPs might contribute to lung damage compared to their larger counterparts [23]. Hence, these NPs may be suitable and have the desired effect on lung cancer cells.

The zeta potential values for AgCS, AgCS-CIS, and AgCS-CIS-SCRBD were positive and greater than 15mV, suggesting good colloidal stability. Zeta potential is an independent property that reflects the surface charge of NPs. It measures colloidal particle stability in an aqueous solution [44,45]. The addition of the cationic chitosan led to a change in the zeta potential of the AgNPs from -30.8 to +20.3, confirming the successful conjugation of chitosan

to the AgNPs. Acceptable zeta potential values are >+30mV or <-30mV, indicating NPs' better dispersion due to the repulsive forces between the NPs [28,46]. However, zeta potential values >-15mV or <15mV will experience aggregation due to forces of attraction that exceed forces of repulsion between the NPs [46]. Hence, the zeta potential value of -30.8mV for the unmodified AgNPs indicates good colloidal stability. The zeta potential values for AgCS, AgCS-CIS, and AgCS-CIS-SCRBD are all positive and greater than 15mV, indicating good, monodispersed NPs with sufficient repulsion forces between them. The slight drop in the zeta potential for AgCS-CIS from +22.8mV to +21.1mV upon ligand binding may be due to anionic charges present within the ligand and the possible masking of some of the chitosan's cationic charges by the ligand.

The AgNPs, AgCS-CIS, and AgCS-CIS-SCRBD had PDI values < 0.4, indicating somewhat dispersed particles. This decreased to 0.183 upon the chitosan conjugation, suggesting an improved dispersity, as confirmed by TEM. The PDI measures the distribution of particle size populations within a sample. PDI values ranging from 0.0 to 1.0 indicate a perfectly uniform to a highly polydisperse sample with multiple particle size populations [47,48]. PDI values within a range of 0.1 to 0.4 indicate highly polydisperse and moderately dispersed particle size distributions [49], as seen in this study.

3.4. Drug encapsulation efficiency.

UV-vis spectroscopy was utilized to determine cisplatin's encapsulation efficiency (EE) by AgCS-CIS and AgCS-CIS-SCRBD. The AgCS-CIS nanocomplex had a high cisplatin EE of 82%, while the AgCS-CIS-SCRBD nanocomplex had a slightly lower EE of 61%. Sodium tripolyphosphate (TPP) played an essential role as a cross-linking agent. Due to the opposing charges (positive/negative) present in the solution, the ionic gelation process was initiated, forming the chitosan-TPP matrix [50,51]. This matrix aided in the entrapment of the cisplatin molecules within the nanocomplex. The difference in encapsulation efficiency between AgCS-CIS and AgCS-CIS-SCRBD could be attributed to the conjugation of the SCRBD with chitosan, leading to fewer chitosan chains available to encapsulate the drug molecules.

3.5. Drug release studies.

Drug release studies evaluated the rate at which the AgCS-CIS (Figure 4A) and AgCS-CIS-SCRBD (Figure 4B) nanocomplexes released the CIS drug payload over a 72-h period under varying pH environments of 4.5, 6.0, and 7.4. For the AgCS-CIS nanocomplex, approximately 32% of the drug was released at pH 4, 26% at pH 6.0 and 7.4 after 30 hours. At pH 4.5, 6.0, and 7.4, a maximum of 96%, 86%, and 78% of the drug were released after 72 hours, respectively. For the AgCS-CIS-SCRBD nanocomplex, approximately 92% of the drug was released at pH 4.5, 79% at pH 6.0, and 58% at pH 7.4 after 72 hours. A 50% drug release was noted after 54 hours at pH 4.5, 60 hours at pH 6.0, and 66 hours at pH 7.4. The improved drug release under acidic environments suggests that these nanocomplexes are pH dependent, which could have been induced by the chitosan polymer, which traps the drug molecules within its matrix and releases them under specific pH conditions.

Chitosan is a weak base, soluble in acidic aqueous solutions with a pH<6.5 [52-54]. This improved drug release under acidic environments because the chitosan matrix that

entrapped the drug solubilized faster, releasing more drug molecules. These findings were similar to those reported in the previous studies for cisplatin release [25,34].

3.6. MTT cytotoxicity assay.

This simple colorimetric assay determines the number of viable cells present after treatment with a compound of interest based on the mitochondrial activity of viable cells [55,56]. Viable cells reduce the MTT reagent (a yellow tetrazolium salt) into insoluble blue formazan crystals, and the number of viable cells is directly proportional to the amount of formazan crystals produced [57]. DMSO is used to solubilize the formazan crystals, which are measured colorimetrically at 540-570nm. Figure 4 illustrates the cytotoxicity profiles of cisplatin, AgNPs, and the nanocomplexes in the HEK293 and A549 cells. The control represents 100% cell viability, and any decrease indicates the levels of cytotoxicity exhibited by the nanocomplexes.

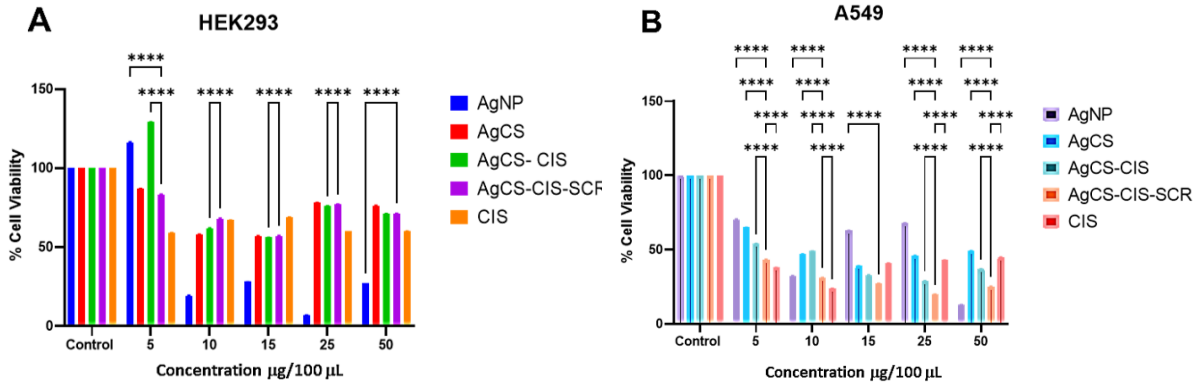

Figure 4. MTT cytotoxicity assay of AgNPs, AgCS, AgCS-CIS, AgCS-CIS-SCRBD, and free cisplatin in **(A)** HEK293; **(B)** A549 cells, cultured in 100µL medium over 48 hours. The data are represented as means ± SD (n=3), ****p<0.0001 were considered statistically significant.

In the HEK293 cells (Figure 4A), the nanocomplexes induced more significant cytotoxicity at 10 and 15µg/100µL than the free drug, cisplatin, which displayed a similar degree of cell death at all concentrations. In both cases, the maximum cell death was around 40%. Since the HEK293 cells were used as healthy, non-cancer cells, these results are important to develop a drug delivery system specific to cancer cells, with little or no cytotoxicity to healthy cells. For the drug-encapsulated nanocomplexes (AgCS-CIS and AgCS-CIS-SCRBD), better cell viability than the free drug was evident at the higher (25µg/100µL and 50µg/100µL) and the lower (5µg/100µL) concentrations tested. This suggested that encapsulation of the drug by the NP aided in reducing the drug's toxicity in normal cells. The cell viability of the AgCS-CIS and AgCS-CIS-SCRBD can be correlated to their pH-dependent nature, which resulted in the release of approximately 40% of cisplatin over 48 hours at a pH of 7.4 in the HEK293 cells. At concentrations of 10µg/100µL and 15µg/100µL, the AgCS nanocomplexes do not exhibit more than 40% of cell death in HEK293 cells. However, the cytotoxicity is reduced at around 25µg/100µL concentrations, suggesting that the nanocomplexes were tolerated by the HEK293 cells.

The AgNPs were cytotoxic (>50% cell death at 10µg/100µL) and showed more significant toxicity than the free cisplatin. It was reported that spherical AgNPs exhibit higher cytotoxicity due to their sizeable volume-to-surface ratio [58]. However, upon modification with chitosan, this toxicity was significantly reduced. This could be attributed to favorable properties, including non-toxicity and biocompatibility. Studies have shown that chitosan-

coated NPs are less toxic than their uncoated counterparts [59]. Previous studies have reported similar results in line with the increased cytotoxicity of AgNPs on HEK293 cells, which was concentration-dependent [60,61]. In earlier studies, Wang and coworkers (2015) proposed that the cause of AgNP cytotoxicity was due to the transformation of Ag^0 to Ag^+, Ag-O-, and Ag-S-, which can cause biochemical changes in cells [62].

In the A549 lung cancer cells (Figure 4 B), a similar increase in the nanocomplex concentration decreased cell viability. The free drug exhibited a high level of cytotoxicity at all concentrations, with approximately 60% cell death. Xie and colleagues showed that the free-form cisplatin administration at concentrations of 3, 6, and 9µg/mL exhibited approximately 10 to 40% of cell death in lung cancer cells [63]. Encapsulating the free drug in nanocomplexes that specifically target the A549 lung cancer cells increased the drug's activity, as seen for the AgCS-CIS-SCRBD nanocomplex. The AgCS-CIS-SCRBD nanocomplex exhibited approximately 60% cell death at the lowest concentration of 5µg/100µL, which increased to 80% as the concentration increased. This highlights the target-specific nature of the AgCS-CIS-SCRBD nanocomplex to the A549 cells.

Cell death obtained by the AgCS-CIS-SCRBD nanocomplex was approximately 10 to 20% higher than that of the non-targeting AgCS-CIS nanocomplex. Importantly, the AgCS-CIS-SCRBD nanocomplexes were more cytotoxic to the A549 than the HEK293 cells. This could be attributed to the increased expression of the ACE2 receptor on the A549 cells [9,64,65] and not in the HEK293 cells. The ACE2 receptor has been abundantly found in the lung epithelium and the small intestine in humans [66]. The AgCS-CIS-SCRBD nanocomplex contains the SCRBD ligand to target the ACE2 receptor and internalizes the nanocomplex by receptor-mediated endocytosis. Although the reduction or silencing of ACE2 expression using therapeutics such as estradiol in A549 cells has been studied [67], anticancer drug targeting via this receptor has not been exploited.

The unmodified AgNPs displayed significant cytotoxicity at a concentration of 50µg/100µL with approximately 90% cell death, while at lower concentrations, they exhibited about 30% cell death. They also showed high cell death in the HEK293 cells, suggesting that using AgNPs in their unmodified form may not be favorable due to the significant toxicity in healthy cells. The AgCS nanocomplexes, on the other hand, displayed higher cytotoxicity in the A549 lung cancer cells than in the HEK293 cells. These results compare favorably with those reported by Huang et al. (2004), who showed the cytotoxic nature of chitosan on A549 cells at concentrations higher than 0.741mg/mL [68]. However, several other studies have used similar concentrations of AgNPs in cytotoxicity evaluations [23], with some upper limits around 1mg/mL [69]. The concentrations used in our study were in keeping with similar in vitro studies reported [25,34].

3.7. Receptor competition binding assay.

The receptor competition binding assay was employed to confirm the capability of the AgCS-CIS-SCRBD nanocomplex to enter the A549 cells via receptor mediation. Uncomplexed SCRBD was utilized as a competitor for the ACE2 receptors. A comparison between cells incubated with the competitor versus cells without the competitor was used to assess the cell viability upon treatment with the AgCS-CIS-SCRBD nanocomplex. The concentrations (25 and 50µg/100µL) that demonstrated the highest levels of cytotoxicity were

employed for this assay. Figure 5 shows that cells incubated with the competitor have higher cell viability than cells not treated with the competitor before the assay.

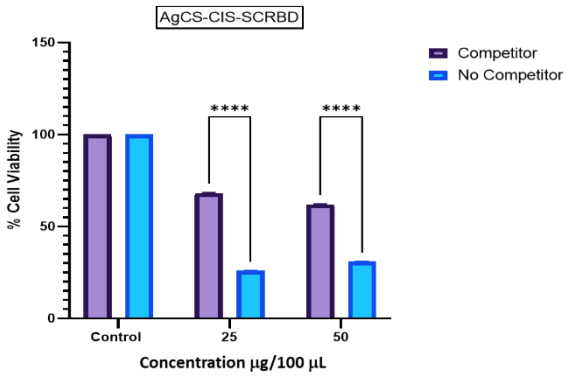

Figure 5. Receptor competition assay in A549 cells using targeted nanocomplexes at concentrations of 25 and 50µg/100µL. The data are represented as means ± SD (n=3), ****p<0.0001 was considered statistically significant.

Cells not treated with the ligand competitor had approximately 30% cell viability, while cells pre-treated with the ligand competitor exhibited 60–70% cell viability. This considerable variation in viability is due to the blockage of the ACE2 receptors upon pre-treatment with excess ligands. The excess ligands bind to their cognate receptors on the A549 cells, preventing the targeted nanocomplexes from receptor-binding and internalizing. This reduced any cytotoxicity that the targeting AgCS-CIS-SCRBD nanocomplex would have had on the cells. These results confirm that the cytotoxicity displayed by AgCS-CIS-SCRBD nanocomplex in the A549 cells largely depended on the uptake of the nanocomplexes via receptor-mediated endocytosis. The formulation of targeting nano-drug delivery systems that utilize the receptor-mediation process has been reported in various studies using organic and inorganic or metal NPs [25,70,71].

3.8. Apoptosis assay.

Most anticancer therapeutics seek to destroy cancer cells by inducing apoptosis, a programmed cell death that can be activated by various factors or signaling pathways [72]. The apoptotic potential of the free drug, AgCS-CIS, and AgCS-CIS-SCRBD were assessed in the A549 cells using their IC50 values derived from the cytotoxicity study. The dual dye system of acridine orange and ethidium bromide (AO/EB) was employed to allow for fluorescent imaging of the cells at various stages of cell death. Fluorescent imaging assists in observing the morphological changes within the cells based on the stage of apoptosis or necrosis. Significant morphological changes observed due to the mechanisms of apoptosis include cell shrinkage, DNA fragmentation, blebbing, the formation of an apoptotic body, and condensation of nuclear chromatin [73]. The permeation of acridine orange into living cells yields a bright green fluorescence, while ethidium bromide stains apoptotic cells yellow-to-red depending on the apoptotic stage of the cell. A lighter green to yellow fluorescence is often observed for early apoptotic cells with fragmented chromatin, while a yellow to orange hue indicates late apoptotic cells with condensed chromatin. An orange-to-red fluorescence with no chromatin condensation indicates necrotic cells [46,74, 75]. The images obtained after treatment with the nano-complexes are shown in Figure 6.

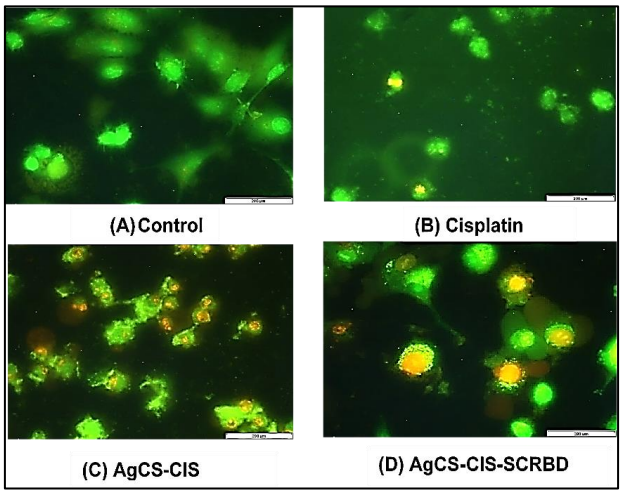

Figure 6. Apoptosis images of A549 cells **(A)** Control; **(B)** Cisplatin; **(C)** AgCS-CIS; **(D)** AgCS-CIS-SCRBD. Scale bar = 200µm.

From Figure 6A, it can be observed that there were no signs of apoptosis in the control (untreated cells). The free drug cisplatin (Figure 6B) showed evidence of both early and late apoptosis, with most of the cells undergoing early apoptosis. There was a high degree of apoptosis for AgCS-CIS (Figure 6C), with most cells showing signs of late apoptosis. Cells treated with the AgCS-CIS-SCRBD nanocomplexes (Figure 6D) exhibited early and late apoptosis with some signs of necrosis. Necrosis is a pathological and inflammatory form of cell death known to be irreversible. It is distinct from apoptosis and transpires when the disruption of the plasma membrane leads to intracellular protein spillage that triggers a damage response resulting in cellular death [76]. The cisplatin-encapsulated nanocomplexes displayed improved apoptotic potential compared to the free drug, as confirmed by their higher apoptotic indices (Table 2).

Table 2. IC50 values and Apoptotic indices for Cisplatin, AgCS-CIS, and AgCS-CIS-SCRBD in A549 cells.

Treatments	Cisplatin	AgCS-CIS	AgCS-CIS-SCRBD
IC50 Values	3µg/100µL	6µg/100µL	2.4µg/100µL
Apoptotic indices	0.8	1	0.9

Some morphological changes were observed in the treated cells, with cells appearing rounded and slightly shortened. It was proposed that exposure of cells to AgNPs can lead to the generation of reactive oxygen species (ROS), DNA damage, inflammation, and increased levels of phosphorylated c-Jun NH2-terminal kinases involved in stress signaling pathways. These factors contribute to the induction of apoptosis [23]. Despite an earlier proposal that AgNPs produce Ag^+, which causes cell death, a recent study has found that cells tolerate AgNPs and Ag^+ differently. Cells exposed to AgNPs underwent lipid peroxidation, leading to proteotoxicity and necrosis, while cells exposed to Ag^+ exhibited oxidative stress and eventual apoptosis [77]. Hence, much is still to be studied on the apoptotic mechanisms induced by AgNPs and their nanocomplexes on mammalian cells before it can be extended to *in vivo* applications. Overall, the apoptosis study correlates to the findings of the cytotoxicity assay.

5. Conclusions

The development of novel approaches to treat lung cancer in the hope of reducing the mortality rate is a significant challenge. Nanomedicine has the impetus to create personalized

and potent therapies through improved nano-drug delivery systems instead of conventional chemotherapies. Incorporating targeting moieties (ligands) in nano-drug delivery systems provides an innovative approach to creating more target-specific cancer treatments. Ligands can specifically target receptors unique to a type of cancer and effectively deliver anticancer drugs to the desired tumor site with high therapeutic indices. This study highlights the targeted delivery of cisplatin to A549 lung cancer cells using chitosan functionalized AgNPs decorated with the targeting ligand, SCRBD, for ACE2 receptor-mediated delivery to lung cancer (A549) cells in vitro. Results obtained from this study have demonstrated the immense potential of the targeting nanocomplex (AgCS-CIS-SCRBD), which exhibited a significant improvement in cytotoxicity over the non-targeting nanocomplex (AgCS-CIS) and two-fold increased cytotoxicity over free cisplatin. The AgCS-CIS-SCRBD nanocomplexes displayed adequate size (<150 nm), dispersion, and stability (>15 mV) with reduced cytotoxicity in healthy HEK293 cells, inferring their potential as a safe and effective targeted delivery system. In addition, we have confirmed that the AgCS-CIS-SCRBD nanocomplex was successfully taken up by the A549 cells via receptor-mediated endocytosis. This targeted nanocomplex formulation has laid the foundation upon which a suitable delivery system to target lung cancer cells can be built. Further investigations and optimizations, in vitro and in vivo, are needed to improve the nanocomplex's stability, size, and cellular uptake.

Funding

This research was funded by the National Research Foundation (NRF), South Africa (Grant numbers: 120455 and 12963).

Acknowledgments

The authors acknowledge Nano-Gene and Drug Delivery Laboratory members for advice and technical assistance.

Conflicts of Interest

The authors declare no conflict of interest.

References

1. Mamdani, H.; Matosevic, S.; Khalid, A.B.; Durm, G.; Jalal, S.I. Immunotherapy in Lung Cancer: Current Landscape and Future Directions. *Front. Immunol.* **2022**, *13*, 823618, https://doi.org/10.3389/fimmu.2022.823618.
2. Sung, H.; Ferlay, J.; Siegel, R.L.; Laversanne, M.; Soerjomataram, I.; Jemal, A.; Bray, F. Global Cancer Statistics 2020: GLOBOCAN Estimates of Incidence and Mortality Worldwide for 36 Cancers in 185 Countries. *CA Cancer J. Clin*. **2021**, *71*, 209–249, https://doi.org/10.3322/caac.21660.
3. Luo, G.; Zhang, Y.; Etxeberria, J.; Arnold, M.; Cai, X.; Hao, Y.; Zou, H. Projections of Lung Cancer Incidence by 2035 in 40 Countries Worldwide: Population-Based Study. *JMIR Public Health Surveill*. **2023**, *9*, e43651, https://doi.org/10.2196/43651.
4. Magrone, T.; Magrone, M.; Jirillo, E. Focus on Receptors for Coronaviruses with Special Reference to Angiotensin- Converting Enzyme 2 as a Potential Drug Target - A Perspective. *Endocr. Metab. Immune. Disord. Drug Targets* **2020**, *6*, 807-811, https://doi.org/10.2174/1871530320666200427112902.
5. Gottschalk, G.; Knox, K.; Roy, A. ACE2: At the crossroad of COVID-19 and lung cancer. *Gene Rep*. **2021**, *23*, 101077, https://doi.org/10.1016/j.genrep.2021.101077.

6. Zhang, H.; Quek, K.; Chen, R.; Chen, J.; Chen, B. Expression of the SAR2-CoV-2 receptor ACE2 reveals the susceptibility of COVID-19 in non-small cell lung cancer. *J. Cancer* **2020**, *11*, 5289-5292, https://doi.org/10.7150/jca.49462.
7. Sivalingam, D.; Singh, M. Targeting the ACE2 receptor using nanomedicine: Novel approach to lung cancer therapy. *Trend Immonother.* **2023**, *7*, 1838, https://doi.org/10.24294/ti.v7.i1.1838.
8. Chai, P.; Yu, J.; Ge, S.; Jia, R.; Fan, X. Genetic alteration, RNA expression, and DNA methylation profiling of coronavirus disease 2019 (COVID-19) receptor ACE2 in malignancies: a pan-cancer analysis. *J. Hematol. Oncol.* **2020**, *13*, 43, https://doi.org/10.1186/s13045-020-00883-5.
9. Pinto, B.G.G.; Oliveira, A.E.R.; Singh, Y.; Jimenez, L.; Gonçalves, A.N.A.; Ogava, R.L.T.; Creighton, R.; Peron, J.P.S.; Nakaya, H.I. ACE2 Expression Is Increased in the Lungs of Patients With Comorbidities Associated With Severe COVID-19. *J. Infect. Dis*. **2020**, *222*, 556-563, https://doi.org/10.1093/infdis/jiaa332.
10. Qian, Y.-R.; Guo, Y.; Wan, H.-Y.; Fan, L.; Feng, Y.; Ni, L.; Xiang, Y.; Li, Q.-Y. Angiotensin-converting enzyme 2 attenuates the metastasis of non-small cell lung cancer through inhibition of epithelial-mesenchymal transition. *Oncol. Rep.* **2013**, *29*, 2408-2414, https://doi.org/10.3892/or.2013.2370.
11. Cheng, Q.; Zhou, L.; Zhou, J.; Wan, H.; Li, Q.; Feng, Y. ACE2 overexpression inhibits acquired platinum resistance-induced tumor angiogenesis in NSCLC. *Oncol. Rep.* **2016**, *36*, 1403-1410, https://doi.org/10.3892/or.2016.4967.
12. Yu, C.; Tang, W.; Wang, Y.; Shen, Q.; Wang, B.; Cai, C.; Meng, X.; Zou, F. Downregulation of ACE2/Ang-(1–7)/Mas axis promotes breast cancer metastasis by enhancing store-operated calcium entry. *Cancer Lett.* **2016**, *376*, 268-277, https://doi.org/10.1016/j.canlet.2016.04.006.
13. Ghosh, P.; Han, G.; De, M.; Kim, C.K.; Rotello, V.M. Gold nanoparticles in delivery applications. *Adv. Drug Deliv. Rev.* **2008**, *60*, 1307-1315, https://doi.org/10.1016/j.addr.2008.03.016.
14. Chehrehgosha, M.; Khoshnevisan, K.; Maleki, H.; Baharifar, H.; Meftah, A.M.; Sajjadi-Jazi, S.M.; Sharifi, F. A systematic study of nano-based fibrous systems: Diagnostic and therapeutic approaches for dementia control. *Ageing Res. Rev.* **2023**, *85*, 101853, https://doi.org/10.1016/j.arr.2023.101853.
15. Torchilin V.P. Passive and Active Drug Targeting: Drug Delivery to Tumors as an Example. In Drug Delivery. Handbook of Experimental Pharmacology, Schäfer-Korting M., Eds.; Springer, Berlin, Heidelberg. **2010**, Volume 197, 3-53, https://doi.org/10.1007/978-3-642-00477-3_1.
16. Lee, S.H.; Jun, B.-H. Silver Nanoparticles: Synthesis and Application for Nanomedicine. *Int. J. Mol. Sci.* **2019**, *20,* 865, https://doi.org/10.3390/ijms20040865.
17. Ferdous, Z.; Nemmar, A. Health Impact of Silver Nanoparticles: A Review of the Biodistribution and Toxicity Following Various Routes of Exposure. *Int. J. Mol. Sci.* **2020**, *21*, 2375, https://doi.org/10.3390/ijms21072375.
18. Liao, C.; Li, Y.; Tjong, S.C. Bactericidal and Cytotoxic Properties of Silver Nanoparticles. *Int. J. Mol. Sci.* **2019**; *20*, 449, https://doi.org/10.3390/ijms20020449.
19. Marinho, C.S.; Matias, M.V.F.; Toledo, E.K.M.; Smaniotto, S.; Ximenes-da-Silva, A.; Tonholo, J.; Santos, E.L.; Machado, S.S.; Zanta, C.L.P.S. Toxicity of silver nanoparticles on different tissues in adult *Danio rerio*. *Fish Physiol. Biochem.* **2021**, *47*, 239-249, https://doi.org/10.1007/s10695-020-00909-2.
20. Noorbazargan, H.; Amintehrani, S.; Dolatabadi, A.; Mashayekhi, A.; Khayam, N.; Moulavi, P.; Naghizadeh, M.; Mirzaie, A.; Mirzaie rad, F.; Kavousi, M. Anticancer & anti-metastasis properties of bioorganic-capped silver nanoparticles fabricated from *Juniperus chinensis* extract against lung cancer cells. *AMB Express* **2021**, *11*, 61, https://doi.org/10.1186/s13568-021-01216-6.
21. Sánchez-Salcedo, S.; García, A.; González-Jiménez, A.; Vallet-Regí, M. Antibacterial effect of 3D printed mesoporous bioactive glass scaffolds doped with metallic silver nanoparticles. *Acta Biomater.* **2023**, *155*, 654-666, https://doi.org/10.1016/j.actbio.2022.10.045.
22. Perumal, S.; Atchudan, R.; Ramalingam, S.; Aldawood, S.; Devarajan, N.; Lee, W.; Lee, Y.R. Silver nanoparticles loaded graphene-poly-vinylpyrrolidone composites as an effective recyclable antimicrobial agent. *Environ. Res.* **2023**, *216*, 114706, https://doi.org/10.1016/j.envres.2022.114706.
23. Xu, L.; Wang, Y.-Y.; Huang, J.; Chen, C.-Y.; Wang, Z.-X.; Xie, H. Silver nanoparticles: Synthesis, medical applications, and biosafety. *Theranostics* **2020**, *10*, 8996-9031, https://doi.org/10.7150/thno.45413.
24. Tyagi, P.K.; Mishra, R.; Khan, F.; Gupta, D.; Gola, D. Antifungal Effects of Silver Nanoparticles Against Various Plant Pathogenic Fungi and its Safety Evaluation on *Drosophila melanogaster*. *Biointerf. Res. Appl. Chem.* **2020**, *10*, 6587-6596, https://doi.org/10.33263/BRIAC106.65876596.
25. Veerappan, R.; Daniels, A.; Singh, M. Polymeric Silver Nanoparticles: Potential for Folate-Targeted Delivery of Cisplatin *In Vitro*. *Int. J. Nanosci.* **2021**, *20*, 2150041, https://doi.org/10.1142/S0219581X21500411.

26. Ahsan, S.M.; Thomas, M.; Reddy, K.K.; Sooraparaju, S.G.; Asthana, A.; Bhatnagar, I. Chitosan as biomaterial in drug delivery and tissue engineering. *Int. J. Biol. Macromol.* **2018**, *110*, 97-109, https://doi.org/10.1016/j.ijbiomac.2017.08.140.
27. Wang, W.; Meng, Q.; Li, Q.; Liu, J.; Zhou, M.; Jin, Z.; Zhao, K. Chitosan Derivatives and Their Application in Biomedicine. *Int. J. Mol. Sci*. **2020**, *21*, 487, https://doi.org/10.3390/ijms21020487.
28. Akinyelu, J.; Singh, M. Folate-tagged chitosan-functionalized gold nanoparticles for enhanced delivery of 5-fluorouracil to cancer cells. *Appl. Nanosci*. **2019**, *9*, 7-17, https://doi.org/10.1007/s13204-018-0896-4.
29. Shafabakhsh, R.; Yousefi, B.; Asemi, Z.; Nikfar, B.; Mansournia, M.A.; Hallajzadeh, J. Chitosan: A compound for drug delivery system in gastric cancer-a review. *Carbohydr. Polym*. **2020**, *242*, 116403, https://doi.org/10.1016/j.carbpol.2020.116403.
30. Turkevich, J.; Stevenson, P.C.; Hiller, J. A study of the nucleation and growth processes in the synthesis of colloidal gold. *Discuss. Faraday Soc.* **1951**, *11*, 55–75, https://doi.org/10.1039/df9511100055.
31. Guzman, M.; Dille, J.; Godet, S. Synthesis and antibacterial activity of silver nanoparticles against gram-positive and gram-negative bacteria. *Nanomed.: Nanotechnol. Biol. Med.* **2012**, *8*, 37-45, https://doi.org/10.1016/j.nano.2011.05.007.
32. Gopinath, K.; Gowri, S.; Arumugam, A. Phytosynthesis of silver nanoparticles using *Pterocarpus santalinus* leaf extract and their antibacterial properties. *J. Nanostr. Chem.* **2013**, *3*, 68, https://doi.org/10.1186/2193-8865-3-68.
33. Eskandari, V.; Sahbafar, H.; Zeinalizad, L.; Mahmoudi, R.; Karimpour, F.; Hadi, A.; Bardania, H. Coating of silver nanoparticles (AgNPs) on glass fibers by a chemical method as plasmonic surface-enhanced Raman spectroscopy (SERS) sensors to detect molecular vibrations of Doxorubicin (DOX) drug in blood plasma. *Arab. J. Chem*. **2022**, *15*, 104005, https://doi.org/10.1016/j.arabjc.2022.104005.
34. Gounden, S.; Daniels, A.; Singh, M. Chitosan-Modified Silver Nanoparticles Enhance Cisplatin Activity in Breast Cancer Cells. *Biointerface Res. Appl. Chem*. **2021**, *11*, 10572-10584, https://doi.org/10.33263/BRIAC113.1057210584.
35. Yasmeen, S.; Kabiraz, M.K.; Saha, B.; Qadir, R.; Gafur, A.; Masum, S. Chromium (VI) Ions Removal from Tannery Effluent using Chitosan-Microcrystalline Cellulose Composite as Adsorbent. *Int Res. J. Pure Appl. Chem*. **2016**, *10*, 1-14, https://doi.org/10.9734/IRJPAC/2016/23315.
36. Azhar, F.F.; Shahbazpour, E.; Olad, A. pH sensitive and controlled release system based on cellulose nanofibers-poly vinyl alcohol hydrogels for cisplatin delivery. *Fibers Polym*. **2017**, *18*, 416-423, https://doi.org/10.1007/s12221-017-6958-5.
37. Ghaferi, M.; Amari, S.; Vivek Mohrir, B.; Raza, A.; Ebrahimi Shahmabadi, H.; Alavi, S.E. Preparation, Characterization, and Evaluation of Cisplatin-Loaded Polybutylcyanoacrylate Nanoparticles with Improved In Vitro and In Vivo Anticancer Activities. *J. Pharm.* **2020**, *13*, 44, https://doi.org/10.3390/ph13030044.
38. Cherian, E.; Rajan, A.; Baskar, G. Synthesis of manganese dioxide nanoparticles using co-precipitation method and its antimicrobial activity. *Int. J. Mod. Sci Technol*. **2016**, *1*, 17-22.
39. Merck. IR spectrum table and Chart. Available at: https://www.sigmaaldrich.com/ZA/en/technical-documents/technical-article/analytical-chemistry/photometry-and-reflectometry/ir-spectrum-table (Accessed 25 November 2022).
40. Silambarasan, S.; Abraham, J. Biosynthesis of silver nanoparticles using the bacteria *Bacillus cereus* and their antimicrobial property. *Int. J. Pharm. Pharm. Sci*. **2012**, *4*, 536-540.
41. Oladimeji, O.; Akinyelu, J.; Singh, M. Co-Polymer Functionalised Gold Nanoparticles Show Efficient Mitochondrial Targeted Drug Delivery in Cervical Carcinoma Cells. *J. Biomed. Nanotechnol*. **2020**, *16,* 853-866, https://doi.org/10.1166/jbn.2020.2930.
42. Foroozandeh, P.; Aziz, A.A. Insight into Cellular Uptake and Intracellular Trafficking of Nanoparticles. *Nanoscale Res. Lett.* **2018**, *13*, 339, https://doi.org/10.1186/s11671-018-2728-6.
43. Rejman, J.; Oberle, V.; Zuhorn, I.S.; Hoekstra, D. Size-dependent internalization of particles via the pathways of clathrin-and caveolae-mediated endocytosis. *Biochem. J.* **2004**, *377*,159–169, https://doi.org/10.1042/BJ20031253.
44. Biriukov D, Fibich P, Předota M. Zeta Potential Determination from Molecular Simulations. *J. Phys. Chem. C* **2020**, *124*, 3159-3170, https://doi.org/10.1021/acs.jpcc.9b11371.
45. Lunardi, C.N.; Gomes, A.J.; Rocha, F.S.; De Tommaso, J.; Patience, G.S. Experimental methods in chemical engineering: Zeta potential. *Can. J. Chem. Eng.* **2021**, *99*, 627-639, https://doi.org/10.1002/cjce.23914.

46. Maney, V.; Singh, M. The Synergism of Platinum-Gold Bimetallic Nanoconjugates Enhances 5-Fluorouracil Delivery in vitro. *Pharmaceutics* **2019**, *11*, 439, https://doi.org/10.3390/pharmaceutics11090439.
47. Clayton, K.N.; Salameh, J.W.; Wereley, S.T.; Kinzer-Ursem, T.L. Physical characterization of nanoparticle size and surface modification using particle scattering diffusometry. *Biomicrofluidics* **2016**, *10*, 054107, https://doi.org/10.1063/1.4962992.
48. Danaei, M.; Dehghankhold, M.; Ataei, S.; Davarani, F.H.; Javanmard, R.; Dokhani, A.; Khorasani, S.; Mozafari, M.R. Impact of Particle Size and Polydispersity Index on the Clinical Applications of Lipidic Nanocarrier Systems. *Pharmaceutics* **2018**, *10*, 57, https://doi.org/10.3390/pharmaceutics10020057.
49. Ardani, H.K.; Imawan, C.; Handayani, W.; Djuhana, D.; Harmoko, A.; Fauzia, V. Enhancement of the stability of silver nanoparticles synthesized using aqueous extract of *Diospyros discolor* Willd. leaves using polyvinyl alcohol. *IOP Conf. Ser.: Mater. Sci. Eng.* **2017**, *188*, 012056, https://doi.org/10.1088/1757-899X/188/1/012056.
50. De-Carvalho, F.G.; Magalhaes, T.C.; Teixeira, N.M.; Gondim, B.L.C.; Carlo, H.L.; dos Santos, R.L.; de Oliveira, A.R.; Denadai, Â.M.L. Synthesis and characterization of TPP/chitosan nanoparticles: Colloidal mechanism of reaction and antifungal effect on *C. albicans* biofilm formation. *Mater. Sci. Eng. C.* **2019**, *104*, 109885, https://doi.org/10.1016/j.msec.2019.109885.
51. Quick Guide: Chitosan Nanoparticles Preparation with Ionic Gelation Method. Available online at: https://chitolytic.com/chitosan-nanoparticles-ionic-gelation/#:~:text=When%20chitosan%20is%20cross%2Dlinked, Method%20for%20 producing%20chitosan%20nanoparticles (Accessed 19 October 2022).
52. Qin, C.; Li, H.; Xiao, Q.; Liu, Y.; Zhu, J.; Du, Y. Water-solubility of chitosan and its antimicrobial activity. *Carbohydr. Polym.* **2006**, *63*, 367-374, https://doi.org/10.1016/j.carbpol.2005.09.023.
53. Roy, J.C.; Salaün, F.; Giraud, S.; Ferri, A.; Chen, G.; Guan, J. Solubility of Chitin: Solvents, Solution Behaviors and Their Related Mechanisms. In Solubility of Polysaccharides, Xu, Z., Eds.; InTechOpen, **2017**, Volume 3, 20-60, http://doi.org/10.5772/intechopen.71385.
54. Pardo-Castaño, C.; Bolaños, G. Solubility of chitosan in aqueous acetic acid and pressurized carbon dioxide-water: Experimental equilibrium and solubilization kinetics. *J. Supercrit. Fluids* **2019**, *151,* 63-74, https://doi.org/10.1016/j.supflu.2019.05.007.
55. Adan, A.; Kiraz, Y.; Baran, Y. Cell Proliferation and Cytotoxicity Assays. *Curr. Pharm. Biotechnol.* **2016**, *17*, 1213-1221, https://doi.org/10.2174/1389201017666160808160513.
56. Abel, S.D.A.; Baird, S.K. Honey is cytotoxic towards prostate cancer cells but interacts with the MTT reagent: Considerations for the choice of cell viability assay. *Food Chem.* **2018**, *241*, 70-78, https://doi.org/10.1016/j.foodchem.2017.08.083.
57. Vinken, M.; Blaauboer, B.J. *In vitro* testing of basal cytotoxicity: Establishment of an adverse outcome pathway from chemical insult to cell death. *Toxicol. In Vitro* **2017**, *39*, 104-110, https://doi.org/10.1016/j.tiv.2016.12.004.
58. Yeasmin, S.; Datta, H.K.; Chaudhuri, S.; Malik, D.; Bandyopadhyay, A. In-vitro anticancer activity of shape controlled silver nanoparticles (AgNPs) in various organ-specific cell lines. *J. Mol. Liq.* **2017**, *242*, 757-766, https://doi.org/10.1016/j.molliq.2017.06.047.
59. Frigaard, J.; Jensen, J.L.; Galtung, H.K.; Hiorth, M. The Potential of Chitosan in Nanomedicine: An Overview of the Cytotoxicity of Chitosan Based Nanoparticles. *Front. Pharmacol.* **2022**, *13*, 880377, https://doi.org/10.3389/fphar.2022.880377.
60. Jiang, X.; Lu, C.; Tang, M.; Yang, Z.; Jia, W.; Ma, Y.; Jia, P.; Pei, D.; Wang, H. Nanotoxicity of Silver Nanoparticles on HEK293T Cells: A Combined Study Using Biomechanical and Biological Techniques. *ACS Omega* **2018**, *3*, 6770-6778, https://doi.org/10.1021/acsomega.8b00608.
61. Liu, X.; Shan, K.; Shao, X.; Shi, X.; He, Y.; Liu, Z.; Jacob, J.A.; Deng, L. Nanotoxic Effects of Silver Nanoparticles on Normal HEK-293 Cells in Comparison to Cancerous HeLa Cell Line. *Int. J. Nanomed.* **2021,** *16*, 753-761, https://doi.org/10.2147/IJN.S289008.
62. Wang, L.; Zhang, T.; Li, P.; Huang, W.; Tang, J.; Wang. P.; Liu, J.; Yuan, Q.; Bai, R.; Li, B.; Zhang, K.; Zhao, Y.; Chen, C. Use of Synchrotron Radiation-Analytical Techniques To Reveal Chemical Origin of Silver-Nanoparticle Cytotoxicity. *ACS Nano.* **2015**, *9*, 6532-6547, https://doi.org/10.1021/acsnano.5b02483.
63. Xie, N.; Liu, Y.-R.; Li, Y.-M.; Yang, Y.-N.; Pan, L.; Wei, Y.-B.; Wang, P.-Y.; Li, Y.-J.; Xie, S.-Y. Cisplatin decreases cyclin D2 expression via upregulating miR-93 to inhibit lung adenocarcinoma cell growth. *Mol. Med. Rep.* **2019**, *20*, 3355-3362, http://doi.org/10.3892/mmr.2019.10566.

64. Zhang, H.; Penninger, J.M.; Li, Y.; Zhong, N.; Slutsky, A.S. Angiotensin-converting enzyme 2 (ACE2) as a SARS-CoV-2 receptor: molecular mechanisms and potential therapeutic target. *Intensive Care Med*. **2020**, *46*, 586-590, https://doi.org/10.1007/s00134-020-05985-9.
65. Yang, J.; Petitjean, S.J.L.; Koehler, M.; Zhang, Q.; Dumitru, A.C.; Chen, W.; Derclaye, S.; Vincent, S.P.; Soumillion, P.; Alsteens, D. Molecular interaction and inhibition of SARS-CoV-2 binding to the ACE2 receptor. *Nat. Commun*. **2020**, *11*, 4541, https://doi.org/10.1038/s41467-020-18319-6.
66. Hamming, I.; Timens, W.; Bulthuis, M.L.C.; Lely, A; Navis, G.; van Goor, H. Tissue distribution of ACE2 protein, the functional receptor for SARS coronavirus. A first step in understanding SARS pathogenesis. *J. Pathol.* **2004**, *203*, 631-637, https://doi.org/10.1002/path.1570.
67. Baristaite, G.; Gurwitz, D. Estradiol reducesACE2 and *TMPRSS2* mRNA levels in A549 human lung epithelial cells. *Drug Develop. Res.* **2022**, *83*, 961–966, https://doi.org/10.1002/ddr.21923.
68. Huang, M.; Khor, E.; Lim, L.-Y. Uptake and Cytotoxicity of Chitosan Molecules and Nanoparticles: Effects of Molecular Weight and Degree of Deacetylation. *Pharm. Res.* **2004**, *21*, 344-353, https://doi.org/10.1023/b:pham.0000016249.52831.a5.
69. El-Sheikh, S.M.A.; Edrees, N.; EL-Sayed, H.; Khamis, T.; Arisha, A.H.; Metwally, M.M.M.; Eleiwa, N.Z.; Galal, A.A.A. Could Cisplatin Loading on Biosynthesized Silver Nanoparticles Improve Its Therapeutic Efficacy on Human Prostate Cancer Cell Line and Reduce Its In Vivo Nephrotoxic Effects? *Biol. Trace Elem. Res.* **2022**, *200*, 582-590, https://doi.org/10.1007/s12011-021-02677-3.
70. Singh, M.; Hawtrey, A.; Ariatti, M. Lipoplexes with biotinylated transferrin accessories: Novel, targeted, serum-tolerant gene carriers. *Int. J. Pharm.* **2006**, *321*, 124-137, https://doi.org/10.1016/j.ijpharm.2006.05.005.
71. Akinyelu, J.; Oladimeji, O.; Daniels, A.; Singh, M. Folate-targeted doxorubicin delivery to breast and cervical cancer cells using a chitosan-gold nano-delivery system. *J. Drug Deliv. Sci. Technol*. **2022**, *67*, 102978, https://doi.org/10.1016/j.jddst.2021.102978.
72. Carneiro, B.A.; El-Deiry, W.S. Targeting apoptosis in cancer therapy. *Nat. Rev. Clin. Oncol.* **2020**, *17*, 395–417, https://doi.org/10.1038/s41571-020-0341-y.
73. Jeong, S.H.; Kim, H.H.; Ha, S.E.; Park, M.Y.; Bhosale, P.B.; Abusaliya, A.; Park, K.I.; Heo, J.D.; Kim, H.W.; Kim, G.S. Flavones: Six Selected Flavones and Their Related Signaling Pathways That Induce Apoptosis in Cancer. *Int. J. Mol. Sci.* **2022**, *23*, 10965, https://doi.org/10.3390/ijms231810965.
74. Dhas, N.L.; Ige, P.P.; Kudarha, R.R. Design, optimization and in-vitro study of folic acid conjugated-chitosan functionalized PLGA nanoparticle for delivery of bicalutamide in prostate cancer. *Powder Technol.* **2015**, *283*, 234-245, https://doi.org/10.1016/j.powtec.2015.04.053.
75. Afsar, T.; Trembley, J.H.; Salomon, C.E.; Razak, S.; Khan, M.R.; Ahmed, K. Growth inhibition and apoptosis in cancer cells induced by polyphenolic compounds of *Acacia hydaspica:* Involvement of multiple signal transduction pathways. *Sci. Rep.* **2016**, *6*, 23077, https://doi.org/10.1038/srep23077.
76. Amaravadi, R.K.; Thompson, C.B. The Roles of Therapy-Induced Autophagy and Necrosis in Cancer Treatment. *Clin. Cancer Res*. **2007**, *13*, 7271-7279, https://doi.org/10.1158/1078-0432.CCR-07-1595.
77. Rohde, M.M.; Snyder, C.M.; Sloop, J.; Solst, S.R.; Donati, G.L.; Spitz, D.R.; Furdui, C.M.; Singh, R. The mechanism of cell death induced by silver nanoparticles is distinct from silver cations. *Part. Fibre Toxicol.* **2021**, *18*, 37, https://doi.org/10.1186/s12989-021-00430-1.